Case Studies in Thermal Engineering 52 (2023) 103774

Contents lists available at ScienceDirect

Case Studies in Thermal Engineering

journal homepage: www.elsevier.com/locate/csite

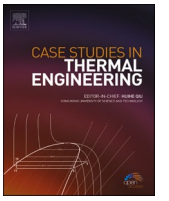

Thermal stability improvement of azobenzene for the integration of photochemical and solar thermochemical energy conversion

Shaopeng Guo [a,b,*], Yanan Zhang [a], Ruifeng Xiong [c], Abhishek Kumar Singh [d]

[a] School of Energy and Environment, Inner Mongolia University of Science and Technology, 014010, Baotou, China
[b] School of Building Services Science and Engineering, Xi'an University of Architecture and Technology, 710055, Xi'an, China
[c] Department of Mechanical, Manufacturing & Biomedical Engineering, Trinity College Dublin, The University of Dublin, D02PN40, Dublin, Ireland
[d] Department of Thermal and Fluid Engineering, University of Twente, 7500, AE Enschede, Netherlands

ARTICLE INFO

Handling Editor: Huihe Qiu

Keywords:
Energy storage
Photochemical energy conversion
Solar thermochemical energy conversion
Thermal stability

ABSTRACT

Azobenzene is a typical photoisomerization material that is widely used in photochemical energy conversion. However, it's generally operated below 200 °C to avoid thermal decomposition. To improve the thermal stability of azobenzene for higher temperature applications, this paper discussed an option that grafting azobenzene onto graphite-like carbon nitride sheets. The synthesis was evaluated based on the performance of micro morphology and structure, thermal stability, and photochemical energy conversion. Furthermore, the photochemical conversion performance was analyzed with diverse irradiation intensities. The results demonstrate that the synthesis has a strong thermal stability below 530 °C. In this study, the most favorable excitation wavelength for photochemical conversion was 445 nm with an irradiation intensity of 40 mW/cm^2.

Nomenclature

Abbreviations

Azo	azobenzene
Azo-1	azobenzene derivative
CNTs	carbon nanotubes
GO	graphene oxide
g-C_3N_4	graphite-like carbon nitride
PES	photoisomerization energy storage
PV	photovoltaic
RGO	reduced graphene oxide

1. Introduction

Solar energy is considered as one of the most promising renewable resources for confronting energy scarcity [1,2]. However, there

* Corresponding author. School of Energy and Environment, Inner Mongolia University of Science and Technology, 014010, Baotou, China.
E-mail address: guoshaopeng@163.com (S. Guo).

https://doi.org/10.1016/j.csite.2023.103774
Received 12 August 2023; Received in revised form 10 November 2023; Accepted 14 November 2023
Available online 17 November 2023

is a growing demand for energy conversion and storage because of the inherent fluctuation and intermittence of solar irradiation [3,4].

The conversion of solar energy to heat is the earliest way that human beings use renewable resource. Concentrated devices such as trough, tower, and dish collectors are commonly used to improve heat flux in the solar thermal conversion process [5,6]. The photovoltaic (PV) effect is responsible for a direct pathway for converting solar energy to electrical energy. However, PV cells can only use solar energy in partial wavelengths due to the semiconductor's band gap energy constraint [7,8]. Solar thermal energy can also be used to run a turbine power generation system, or to drive an endothermic reaction for solar thermochemical energy conversion under near-infrared lights (700–1100 nm) [9–11]. Furthermore, some chemical reactions can be directly induced by light at other wavelengths. For example, ultraviolet and visible light with wavelengths less than 621 nm are used to drive the photochemical conversion of azobenzene [12]. As a result, the integration of photochemical and thermochemical energy conversion could be a promising way to boost the solar energy efficiency across a wide spectrum of solar energy. As shown in Fig. 1, a method of integrating photochemical and solar thermochemical was proposed and evaluated in our previous study [13]. The results demonstrated that the solar energy conversion efficiency was remarkably enhanced.

The most commonly concerned photoresponsive materials are azobenzene, norbornadiene, and anthracene [14]. Among these, azobenzene (Azo) and its derivatives are extremely attractive due to their superiorities such as ease of synthesis, quick response, and high sensitivity, making them a versatile choice for the design of photoswitchable catalysts, photochromic fibers, solar fuels, and so on [14–16]. The unique molecular structure with two phenyl rings joined by an N═N bond allows azobenzene high reactivity to interact with substances such as charged ions via cation-π interaction and the synergistic coordination [17,18]. Furthermore, Azo is an ideal material for solar energy conversion and storage due to its high storage capacity and reversible switching between trans and cis conformation [19]. Even under natural lighting condition, the azobenzene compounds demonstrated 50 % of the *cis*-isomer energy storage within 1–2 h [20]. However, the majority of Azo and its derivatives show poor performances in energy density and half-life of energy storage [21,22]. As such, various methods have been explored to address these challenges. Kolpak et al. [23] successfully grafted Azo onto the carbon nanotubes (CNTs). They discovered that the tighter packing of Azo compounds on CNTs strengthened their intermolecular force, improving their energy density and half-life. Jiang et al. [24] synthesized an Azo-single-walled CNTs hybrid material by employing the direct Friedel-crafts acylation reaction. The synthetic material showed a good performance in energy density (80.7 Wh/kg). However, the unique one-dimensional cylindrical structure of CNTs restricted the energy transfer in the radial direction.

Graphene is a two-dimensional layered structure composed of single atomic layers of carbon atoms linked by SP^2 hybridization, which can effectively solve the abovementioned problem [25]. Feng et al. [26] developed an Azo/graphene hybrid material. The energy density and recovery half-life of the hybrid material reached 269.8 J/g and 5400 h, respectively. Xu et al. [27] grafted Azo onto the graphene oxide (GO) to obtain a hybrid material with a dendritic hyperbranched structure. The energy density of the synthesized material reached 374 J/g, making it nearly three times that of the original Azo. Yan et al. [28] covalently grafted thiazole heterocyclic Azo molecules to the surface of reduced graphene oxide (RGO). The energy density of the synthesized material reached 138 Wh/kg, while the storage half-life was 10 h.

Another major concern with Azo and its derivatives is related to their thermal decomposition when heated up to 200 °C [29,30]. Because most solar thermochemical conversions are operated above 200 °C, the poor thermal stability of Azo and its derivatives limits their application in a solar thermochemical energy system [31,32]. Therefore, a new thermoresistant Azo-based synthesis is required.

Graphite-like carbon nitride (g-C_3N_4) has a six-member conjugated layered structure like graphene [33], and is generally characterized as a graphene framework with the substitution of part nitrogen atoms. The interlayer spacing of g-C_3N_4 is even slightly smaller than that of graphene [34]. Because of this structural advantage, g-C_3N_4 has a large specific surface area, which is beneficial for a high synthesis rate [35]. In addition, the triazine ring structure in g-C_3N_4 has demonstrated a great impact on thermal stability [36,37]. Thus, the existence of g-C_3N_4 may greatly improve the heat resistance of materials. The properties of soluble and chemical stability give g-C_3N_4 a competitive edge in synthesis [38]. Moreover, it also has advantages such as low cost, non-toxicity, and ease of processability and recyclability [39]. Despite g-C_3N_4 has a positive effect on thermal stability, the synthetic method and performance of Azo/g-C_3N_4 material has not to be reported yet. Furthermore, the effect of irradiation densities on Azo/g-C_3N_4 photoisomerization is

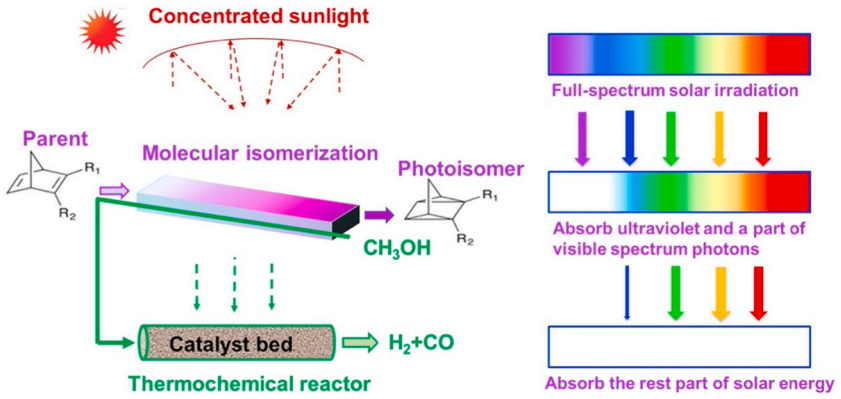

Fig. 1. The concept of integration of photochemical and solar thermochemical energy conversion [13].

unclear.

The goal of this paper is to improve the thermal stability of Azo for the integration of photochemical and solar thermochemical energy conversion. We prepared and evaluated a high thermal stability Azo-based material. The Azo synthesis demonstrated excellent photochemical sensibility and thermal stability, meeting the thermoresistant material requirement for achieving photochemical and solar thermochemical energy conversion integration.

2. Experimental

2.1. Preparation

The preparation of Azo-1/g-C_3N_4 hybrid material follows the route as shown in Fig. 2. It consists of the following three steps.

i) Preparation of g-C_3N_4. The urea was heated at 550 °C in a nitrogen atmosphere for 2 h. Then, the product is naturally cooled to room temperature.

ii) Preparation of Azo-1. First, the diazonium salt solution was prepared by dissolving aniline and $NaNO_2$ in distilled water, and then dropwise adding HCl solution. Second, the 3,5-dimethoxyaniline solution was diluted with diazonium salt solution. Their mixture was fully agitated in an ice bath for 4 h. The crude product of Azo-1 could be obtained at PH 7. Finally, it was purified by chromatography, distillation and vacuum drying at room temperature to obtain the Azo-1 powdery solid.

iii) Preparation of Azo-1/g-C_3N_4. First, the Azo-1 and the $NaNO_2$ were dissolved in 40 mL of deionized water. Second, the mixture was slowly dropped into the HCl solution and reacted in an ice bath for 1 h. Third, the above combination was added into the g-C_3N_4 aqueous solution. The reaction was carried out in an ice bath for 4 h. Then, it stood at room temperature for 12 h. The above mixture was washed with deionized water, acetone, DMF and filtered through a PTFE membrane until no residual Azo-1 was detected by UV–Vis spectroscopy. The preceding procedure was repeated two more times. Finally, the Azo-1/g-C_3N_4 materials were obtained.

2.2. Characterizations

Morphologies of g-C_3N_4 and Azo-1/g-C_3N_4 were observed by scanning electron microscopy (SEM, GAIA3 TESCAN, Brno, Czech Republic). The chemical structure of Azo-1/g-C_3N_4 was investigated using Fourier transform infrared (FT-IR, Bruker Vertex70, Bruker, Germany) spectroscopy. The crystal structure was determined by employing X-ray diffraction (XRD, D8 ADVANCE, Bruker, Germany) patterns with a scanning range from 5 to 90°. The elemental compositions of Azo-1 and Azo-1/g-C_3N_4 were examined by X-ray photoelectron spectroscopy (XPS, ESCALAB Xi+, Thermo Scientific, USA). Thermogravimetric analysis (TGA, 209 F3, NETZSCH, Germany) was performed at temperatures ranging from 30 to 800 °C and a rate of 10 °C/min. The Photoisomerization performance of Azo-1/g-C_3N_4 was evaluated by an ultraviolet–visible (UV–Vis, UV1780, SHIMADZU, Japan) spectrophotometer with a wavelength range of 250–700 nm.

3. Results and discussion

3.1. Micro morphology and chemical structure

The micromorphological features of syntheses are depicted in Fig. 3a. The tangled and porous microstructure of g-C_3N_4 were observed resulting in agglomerates in size of micrometers. The loose and corrugated sheets appeared in g-C_3N_4 can provide a large specific surface area, contributing to a high synthesis activity [40]. Whereas, the surface of Azo-1/g-C_3N_4 became smooth and flat compared to the original g-C_3N_4. The smoother surface may attribute to the covering by the covalent functionalization of Azo-1 groups on the g-C_3N_4 surface. The evidence in surface coating may preliminarily infer the existence of synthesis.

Fig. 2. Schematic illustration for the preparation of Azo-1/g-C_3N_4.

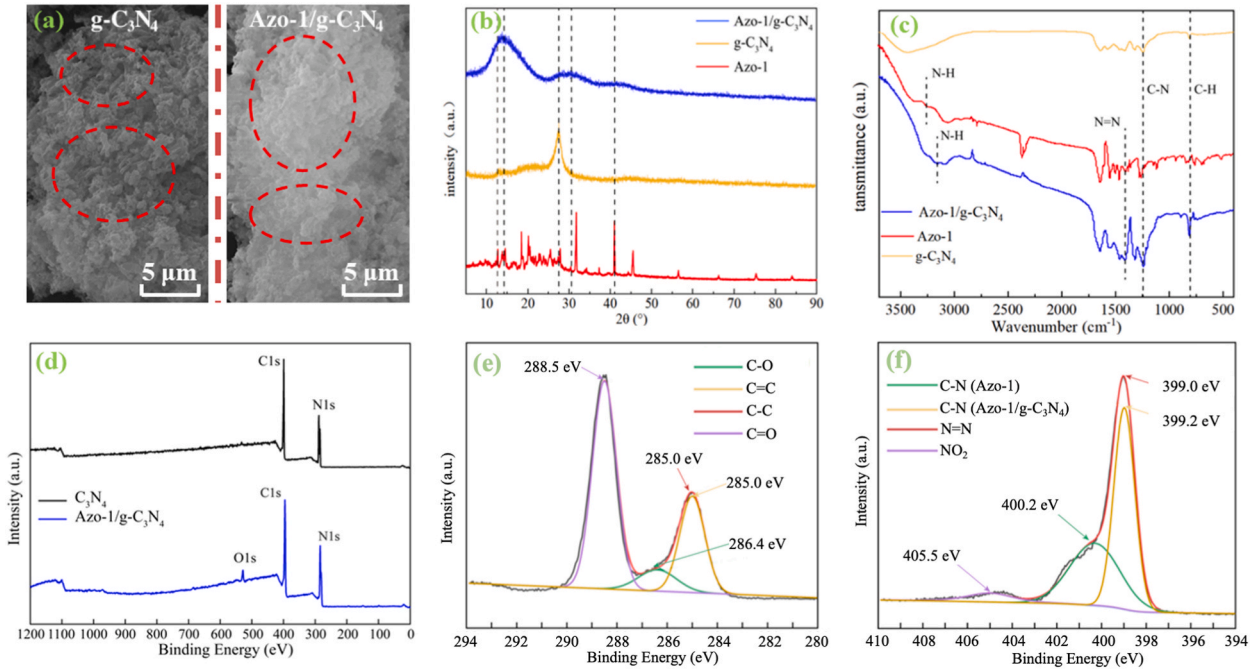

Fig. 3. Micromorphological features and functional groups: (a) SEM images, (b) XRD spectra, (c) FT-IR spectra, (d) XPS spectra, (e) XPS C 1s, (f) XPS N 1s.

Fig. 3b shows the XRD patterns of g-C_3N_4, Azo-1 and Azo-1/g-C_3N_4. The diffraction peak at 12.9° is assigned to (100) crystal phase of g-C_3N_4 with an inter-planar distance of 0.687 nm. While, the diffraction peak at 27.5° is the (002) crystal plane of g-C_3N_4 with the inter-planar distance of 0.325 nm. Moreover, the Azo-1 pattern had more diffraction peaks, indicating that its crystal structure was organized. Three peaks at 14.5°, 31.7° and 40.9° were detected in XRD pattern of Azo-1/g-C_3N_4. These diffraction peaks were possibly caused by the hydrogen bonds on g-C_3N_4 surface as well as the Azo bonds. When the diffraction peaks of Azo-1/g-C_3N_4, Azo-1, and g-C_3N_4 were compared, no additional peaks were discovered. This may also indicate that Azo-1 was successfully grafted onto g-C_3N_4 without breaking the crystal structures of Azo-1 and g-C_3N_4. The above conclusion can be confirmed using FT-IR spectra analysis. As shown in Fig. 3c, the peaks at 779 cm^{-1} and 1460 cm^{-1} in Azo-1 and Azo-1/g-C_3N_4 patterns correspond to the bands of C–H and N═N, respectively. The red shifts of the peaks with respect to C–N (from 1288 cm^{-1} to 1240 cm^{-1}) and N–H (from 3370 cm^{-1} to 3250 cm^{-1}) are observed before and after grafting reaction of Azo-1. No new distinct peak was discovered in FT-IR spectra other than the above characteristic constituents, which indicates that there was no other chemical reaction between Azo-1 and g-C_3N_4 during the synthetic process.

Furthermore, bonding configuration analysis of XPS spectra can reveal additional proof regarding Azo-1 and g-C_3N_4 compatibility. As shown in Fig. 3d, a distinct peak can be observed at around 534 eV with respect to O 1s in the wide XPS spectrum of Azo-1/g-C_3N_4. However, it is absent from the XPS spectrum of g-C_3N_4. The difference of O 1s peak between spectra of Azo-1/g-C_3N_4 and g-C_3N_4 may

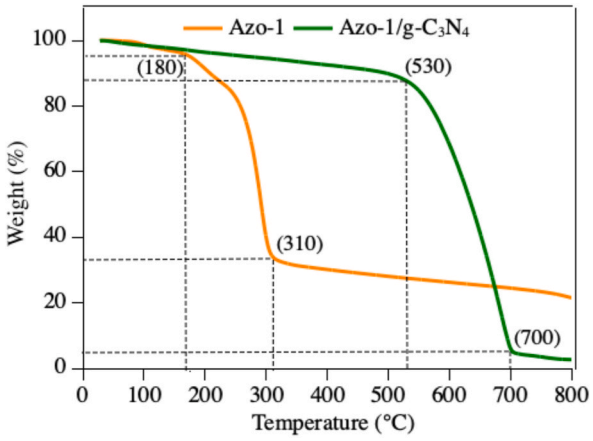

Fig. 4. TGA of Azo-1 and Azo-1/g-C_3N_4.

further indicate the introduction of Azo-1 onto g-C_3N_4 sheets. Meanwhile, the C 1s core level XPS of Azo-1/g-C_3N_4 (Fig. 3e) displays a peak at 285.0 eV corresponding to the carbon framework in the Azo-1 functional group. The C–O and C═O groups are represented by two components centered at 286.4 and 288.5 eV, respectively. The N atoms were most likely derived from three bonds: the N═N bond and C–N in Azo-1, as well as the C–N bond connecting Azo-1 and g-C_3N_4. The N 1s spectra of Azo-1/g-C_3N_4 can be decomposed into three components as shown in Fig. 3f. The two peaks with binding energies 399.0 and 399.2 eV, correspond to the N═N and C–N bonds, respectively. The other two peaks, located at 400.2 eV and 405.5 eV, are characterized by the C–N bond connecting Azo-1 and g-C_3N_4 and NO_2, respectively.

3.2. Thermal stability

Fig. 4 shows the TGA results of Azo-1 and Azo-1/g-C_3N_4. As other Azo derivatives, the Azo-1 performed poorly in thermal stability tests [30,41]. The evaporation of the water physically adsorbed on the surface of Azo-1 resulted in a minor reduction below 180 °C, accounting for about 5 % weight loss. Then, the material's weight decreased significantly between 180 and 310 °C, with approximately 33 % remaining due to the conversion of oxygen-containing groups into CO and CO_2 during thermal degradation [42]. After that, the weight of Azo-1 gradually decreased over 310 °C. The Azo-1/g-C_3N_4 on the other hand, performed exceptionally well in thermal stability tests. Only 12 % of Azo-1/g-C_3N_4 decomposed below 530 °C. Apparently, the distinct change of Azo-1 in heat resistance is attributed to chemical grafting with g-C_3N_4 sheets. Thermal decomposition of original Azo and its derivatives commonly occurs by breaking the bonds beside N═N and forming two free phenyl radicals [43]. Thus, their degradation temperature would be improved depending on the substituted groups and positions in reactions. The inter-and intra-molecular hydrogen bonding between the Azo and nano templates also increased the dissociation energy of bonds [44]. Furthermore, g-C_3N_4 has been known as a most thermal and chemical stable allotrope of carbon nitride due to its 2D tri-*s*-triazine structure [45,46]. The great enhancement of thermal stability makes the Azo-1/g-C_3N_4 competent for most application of low and medium temperature solar energy. However, it lost 83 % of its weight between 530 and 700 °C, indicating that this Azo synthesis is not suitable for high temperature applications.

3.3. Photoisomerization performance

The evaluation of UV–Vis absorption behavior is of the utmost importance for determining photoisomerization energy storage performance. Fig. 5 illustrated the *trans*-to-cis isomerization behaviors of Azo-1/g-C_3N_4 when exposed to UV–Vis light at 365 nm and 50 mW/cm^2. As shown in the UV–Vis absorption spectra, the distinct peaks appear at the wavelength of 445 nm under excitation in trans-Azo moieties. A slight red shift of peaks occurred in Azo-1/g-C_3N_4 spectra due to an increase in the charge transfer character of the π→π* transition across the long axis of the molecule after grafting [47]. The absorbance gradually dropped with the continuous radiation of UV–Vis light due to the *trans*-to-cis isomerization transition of Azo compounds. The characteristic peaks nearly vanished after 300 min, indicating that the majority of Azo moieties have reached the metastable state and completed *trans*-to-cis isomerization.

The inherent fluctuation in solar irradiation intensity is a significant consideration when designing a high-efficiency energy storage material. In general, the irradiation intensities in concentrated solar thermochemical energy systems are below 50 mW/cm^2 [48–52]. To explore the optimal irradiation intensity for the integration of photochemical and solar thermochemical energy conversion, UV–Vis absorption studies were carried out with irradiation intensities of 10, 20, 30, 40, and 50 mW/cm^2.

As shown in Fig. 6, no new red shift of π→π* transition was found in the Azo-1/g-C_3N_4 peaks when compared to those in Fig. 5, meaning good isomerization stability with various irradiation intensities. In summary, the absorbances of Azo-1/g-C_3N_4 decreased as the irradiation intensities boosted because the UV–Vis absorption reactions became more moderate as the amount of remanent unphotoisomerized materials decreased. Consequently, the photoisomerization performance of Azo-1/g-C_3N_4 is more sensitive to higher irradiation intensities. However, this effect becomes weak when the irradiation intensity exceeds 40 mW/cm^2. An irradiation intensity of 40 mW/cm^2 is recommended for the Azo-1/g-C_3N_4 synthesized in this paper.

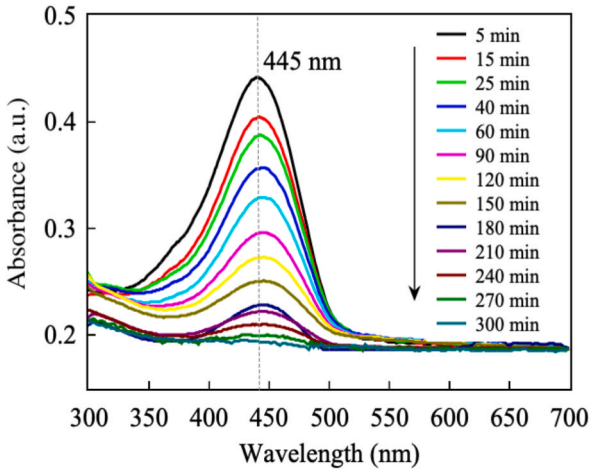

Fig. 5. UV–Vis absorption spectra of Azo-1/g-C_3N_4.

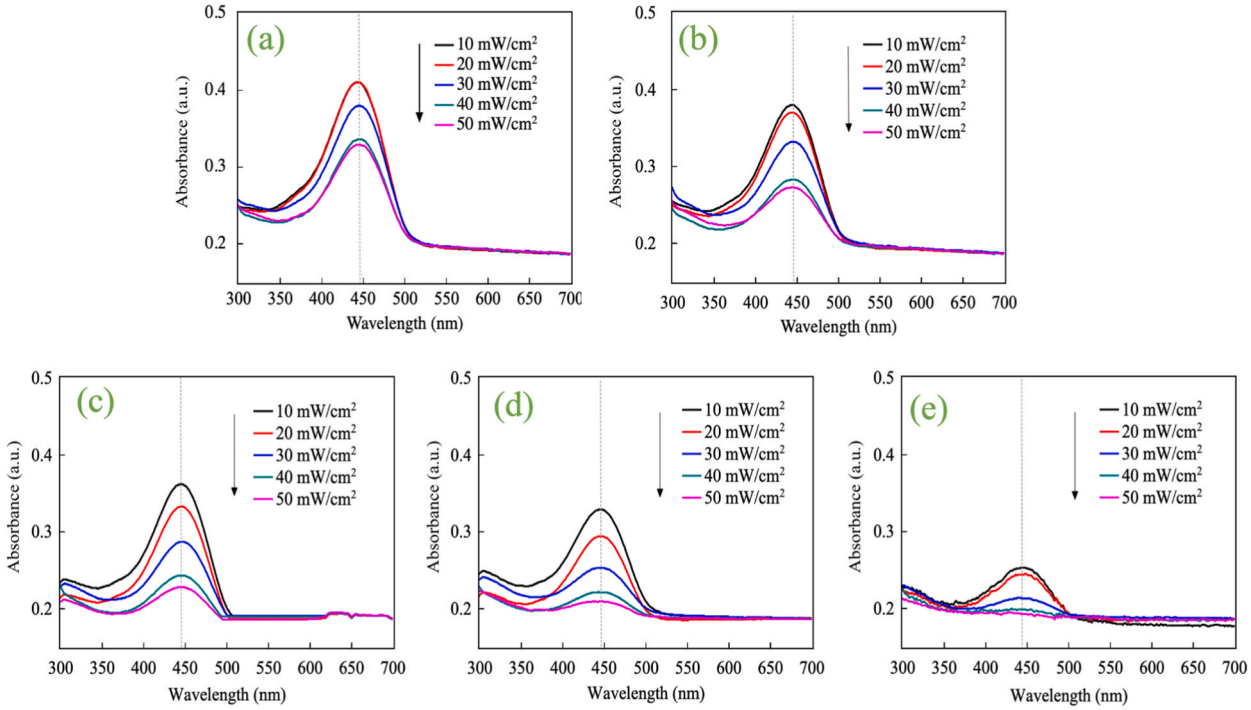

Fig. 6. UV–Vis absorption spectra of Azo-1/g-C_3N_4 with diverse irradiation intensities: (a) 60 min, (b) 120 min, (c) 180 min, (d) 240 min, (e) 300 min.

4. Conclusions

To improve the thermal stability of azobenzene, we synthesized a novel photoisomerization material by grafting Azo-1 on g-C_3N_4 sheets. The micromorphological features, thermal stability, and photoisomerization performance were evaluated based on a series of characterizations. The conclusions can be drawn as follows.

- The synthesis Azo-1/g-C_3N_4 demonstrated a good performance in thermal stability below 530 °C, making it suitable for the majority of low and medium temperature solar energy applications.
- The *trans*-to-cis isomerization of Azo moieties took approximately 300 min when exposed to UV–Vis light at 365 nm and 50 mW/cm^2. A red shift of π→π* transition occurred after grafting. The optimal excitation wavelength for Azo-1/g-C_3N_4 is 445 nm.
- The photoisomerization transition of Azo-1/g-C_3N_4 is more sensitive to higher irradiation intensity. However, the appropriate irradiation intensity is 40 mW/cm^2 for the Azo-1/g-C_3N_4 synthesized in this paper.

Author statement

Shaopeng Guo: Conceptualization, Supervision, Methodology, Funding acquisition, Writing–original draft, Writing–review & editing. **Yanan Zhang**: Analysis, Validation, Writing – review & editing. **Ruifeng Xiong**: Investigation, Data curation. **Abhishek Kumar Singh**: Analysis, Writing–review & editing.

Declaration of competing interest

The authors declare that they have no known competing financial interests or personal relationships that could have appeared to influence the work reported in this paper.

Data availability

Data will be made available on request.

Acknowledgements

This work was supported by the National Natural Science Foundation of China (No. 51966015).

References

[1] E.G. Barbosa, M.E.V.d. Araujo, A.C.L.d. Oliveira, M.A. Martins, Thermal energy storage systems applied to solar dryers: classification, performance, and numerical modeling: an updated review, Case Stud. Therm. Eng. 45 (2023), 102986.

[2] C. Chen, Q. Xia, S. Feng, Q. Liu, A novel solar hydrogen production system integrating high temperature electrolysis with ammonia based thermochemical energy storage, Energy Convers. Manag. 237 (2021), 114143.
[3] V. Kashyap, S. Sakunkaewkasem, P. Jafari, M. Nazari, B. Eslami, S. Nazifi, P. Irajizad, M.D. Marquez, T.R. Lee, H. Ghasemi, Full spectrum solar thermal energy harvesting and storage by a molecular and phase-change hybrid material, Joule 3 (12) (2019) 3100–3111.
[4] P. Lin, J. Xie, Y. He, X. Lu, W. Li, J. Fang, S. Yan, L. Zhang, X. Sheng, Y. Chen, MXene aerogel-based phase change materials toward solar energy conversion, Sol. Energy Mater. Sol. Cell. 206 (2020), 110229.
[5] Y. Bai, L. Wang, L. Lin, X. Lin, L. Peng, H. Chen, A performance analysis of the spray-type packed bed thermal energy storage for concentrating solar power generation, J. Energy Storage 51 (2022), 104187.
[6] X. Zhao, S. Yan, N. Zhang, N. Zhao, H. Gao, Solar flux measuring and optical efficiency forecasting of the linear fresnel reflector concentrator after dust accumulation, J. Therm. Sci. 31 (3) (2022) 663–677.
[7] T. Zhu, Q. Li, A. Yu, Analysis of the solar spectrum allocation in a spectral-splitting photovoltaic-thermochemical hybrid system, Sol. Energy 232 (2022) 63–72.
[8] T. Zhang, J. Cai, W. Zheng, Y. Zhang, Q. Meng, Comparative and sensitive analysis of the annual performance between the conventional and the heat pipe PV/T systems, Case Stud. Therm. Eng. 28 (2021), 101380.
[9] R. Bian, Y. Deng, C. Feng, B. Yu, D. Sun, W. Zhang, Performance and optimization study of graded thermal energy storage system for direct steam generation dish type solar thermal power, Case Stud. Therm. Eng. 49 (2023), 103369.
[10] T. Banerjee, F. Podjaski, J. Kröger, B.P. Biswal, B.V. Lotsch, Polymer photocatalysts for solar-to-chemical energy conversion, Nat. Rev. Mater. 6 (2) (2021) 168–190.
[11] M. Zhang, X. Zhang, K. Zhao, Y. Dong, W. Yang, J. Liu, D. Li, Assembly of gold nanorods with L-cysteine reduced graphene oxide for highly efficient NIR-triggered photothermal therapy, Spectrochim. Acta Mol. Biomol. Spectrosc. 266 (2022), 120458.
[12] G. Ouyang, D. Bialas, F. Würthner, Reversible fluorescence modulation through the photoisomerization of an azobenzene-bridged perylene bisimide cyclophane, Org. Chem. Front. 8 (7) (2021) 1424–1430.
[13] J. Fang, Q. Liu, S. Guo, J. Lei, H. Jin, Spanning solar spectrum: a combined photochemical and thermochemical process for solar energy storage, Appl. Energy 247 (2019) 116–126.
[14] R. Zhao, Y. Li, J. Bai, J. Mu, L. Chen, N. Zhang, J. Han, F. Liu, S. Yan, Preparation of flexible photo-responsive film based on novel photo-liquefiable azobenzene derivative for solar thermal fuel application, Dyes Pigments 202 (2022), 110277.
[15] A.-x. Zheng, C.-b. Gong, W.-j. Zhang, Q. Tang, H.-r. Huang, C.-f. Chow, Q. Tang, An amphiphilic and photoswitchable organocatalyst for the aldol reaction based on a product-imprinted polymer, Mol. Catal. 442 (2017) 115–125.
[16] S. Fan, Y. Lam, J. Yang, X. Bian, J.H. Xin, Development of photochromic poly(azobenzene)/PVDF fibers by wet spinning for intelligent textile engineering, Surface. Interfac. 34 (2022), 102383.
[17] A. Goulet-Hanssens, C.J. Barrett, Photo-control of biological systems with azobenzene polymers, J. Polym. Sci. Polym. Chem. 51 (14) (2013) 3058–3070.
[18] X. Zuo, Y. He, H. Ji, Y. Li, X. Yang, B. Yu, T. Wang, Z. Liu, W. Huang, J. Gou, N. Yuan, J. Ding, S.F. Liu, In-situ photoisomerization of azobenzene to inhibit ion-migration for stable high-efficiency perovskite solar cells, J. Energy Chem. 73 (2022) 556–564.
[19] R. Duan, D. Wu, L. Tang, X. Hu, L. Cheng, H. Yang, H. Li, F. Geng, Interactions of the cis and trans states of an azobenzene photoswitch with lysozyme induced by red and blue light, Spectrochim. Acta Mol. Biomol. Spectrosc. 229 (2020), 117965.
[20] S.L. Barrett, C. Meyer, E. Cwiklik, V. Fieglein, M. Burns, J. Guerrero, W.J. Brittain, Kinetic study of azobenzene photoisomerization under ambient lighting, J. Photochem. Photobiol. Chem., 446 (2024) 115114..
[21] H. Liu, Y. Feng, W. Feng, Alkyl-grafted azobenzene molecules for photo-induced heat storage and release via integration function of phase change and photoisomerization, Compos. Commun. 21 (2020), 100402.
[22] Z. Li, L. Wang, Y. Li, Y. Feng, W. Feng, Carbon-based functional nanomaterials: preparation, properties and applications, Compos. Sci. Technol. 179 (2019) 10–40.
[23] A.M. Kolpak, J.C. Grossman, Azobenzene-functionalized carbon nanotubes as high-energy density solar thermal fuels, Nano Lett. 11 (8) (2011) 3156–3162.
[24] Y. Jiang, J. Huang, W. Feng, X. Zhao, T. Wang, C. Li, W. Luo, Molecular regulation of nano-structured solid-state AZO-SWCNTs assembly film for the high-energy and short-term solar thermal storage, Sol. Energy Mater. Sol. Cell. 193 (2019) 198–205.
[25] M. Li, C. Wang, AAZO-Graphene composite phase change materials with Photo-thermal conversion performance, Sol. Energy 223 (2021) 11–18.
[26] Y. Feng, H. Liu, W. Luo, E. Liu, N. Zhao, K. Yoshino, W. Feng, Covalent functionalization of graphene by azobenzene with molecular hydrogen bonds for long-term solar thermal storage, Sci. Rep. 3 (1) (2013) 3260.
[27] X. Xu, B. Wu, P. Zhang, H. Yu, G. Wang, Molecular solar thermal storage enhanced by hyperbranched structures, Sol. RRL 4 (1) (2020), 1900422.
[28] Q. Yan, Y. Zhang, Y. Dang, Y. Feng, W. Feng, Solid-state high-power photo heat output of 4-((3,5-dimethoxyaniline)-diazenyl)-2- imidazole/graphene film for thermally controllable dual data encoding/reading, Energy Storage Mater. 24 (2020) 662–669.
[29] X. Yang, S. Li, J. Zhao, X. Wang, H. Huang, Y. Wang, Visible light driven low temperature photoactive energy storage materials for high rate thermal output system, Sol. Energy Mater. Sol. Cell. 231 (2021), 111330.
[30] W. Pang, J. Xue, H. Pang, A high energy density azobenzene/graphene oxide hybrid with weak nonbonding interactions for solar thermal storage, Sci. Rep. 9 (1) (2019) 5224.
[31] X. Li, X. Sun, Q. Song, Z. Yang, H. Wang, Y. Duan, A critical review on integrated system design of solar thermochemical water-splitting cycle for hydrogen production, Int. J. Hydrogen Energy 47 (79) (2022) 33619–33642.
[32] D. Li, J. Sun, R. Ma, J. Wei, High-efficient solar-driven hydrogen production by full-spectrum synergistic photo-thermo-catalytic methanol steam reforming with in-situ photoreduced Pt-CuOx catalyst, J. Energy Chem. 71 (2022) 460–469.
[33] E. Vivek, A. Arulraj, M. Khalid, I. Vetha Potheher, Facile synthesis of 2D Ni(OH)2 anchored g-C3N4 as electrode material for high-performance supercapacitor, Inorg. Chem. Commun. 130 (2021), 108704.
[34] J. Safaei, N.A. Mohamed, M.F. Mohamad Noh, M.F. Soh, N.A. Ludin, M.A. Ibrahim, W.N. Roslam Wan Isahak, M.A. Mat Teridi, Graphitic carbon nitride (g-C3N4) electrodes for energy conversion and storage: a review on photoelectrochemical water splitting, solar cells and supercapacitors, J. Mater. Chem. A 6 (45) (2018) 22346–22380.
[35] C. Chen, J. Wang, H. Dong, W. Chen, K. Zhou, Facile synthesis of graphite-like carbon nitride/zinc oxide heterojunction for microwave absorption, J. Alloys Compd. 935 (2023), 167723.
[36] X. Zhang, Q. Chi, C. Tang, H. Li, C. Zhang, Z. Li, T. Zhang, Achieving high-temperature resistance and excellent insulation property of epoxy by introducing triazine ring structure, J. Mater. Sci. Mater. Electron. 34 (7) (2023) 638.
[37] J. Wang, S. Yu, S. Xiao, Research progress of triazine flame retardants, Macromol. Res. 31 (4) (2023) 339–357.
[38] C. Jia, L. Yang, Y. Zhang, X. Zhang, K. Xiao, J. Xu, J. Liu, Graphitic carbon nitride films: emerging paradigm for versatile applications, ACS Appl. Mater. Interfaces 12 (48) (2020) 53571–53591.
[39] Q. Cao, B. Kumru, M. Antonietti, B.V. Schmidt, Graphitic carbon nitride and polymers: a mutual combination for advanced properties, Mater. Horiz. 7 (3) (2020) 762–786.
[40] Z. Durmus, A.W. Maijenburg, A review on graphitic carbon nitride (g-C3N4) – metal organic framework (MOF) heterostructured photocatalyst materials for photo(electro)chemical hydrogen evolution, Int. J. Hydrogen Energy 47 (87) (2022) 36784–36813.
[41] F.A. Jerca, V.V. Jerca, R. Hoogenboom, Advances and opportunities in the exciting world of azobenzenes, Nat. Rev. Chem 6 (1) (2022) 51–69.
[42] A. Amiri, M. Shanbedi, G. Ahmadi, H. Eshghi, S.N. Kazi, B.T. Chew, M. Savari, M.N.M. Zubir, Mass production of highly-porous graphene for high-performance supercapacitors, Sci. Rep. 6 (1) (2016), 32686.
[43] T.L. Nguyen, M.A. Saleh, Thermal degradation of azobenzene dyes, Results in Chemistry 2 (2020), 100085.
[44] A. Baby, S. Abinaya, A.M. John, S.P. Jose, S.P. Balakrishnan, Photoresponse and electrochemical behaviour of azobenzene anchored graphene oxide for energy storage application, Mater. Chem. Phys. 301 (2023), 127592.

[45] Y. Shi, S. Jiang, K. Zhou, C. Bao, B. Yu, X. Qian, B. Wang, N. Hong, P. Wen, Z. Gui, Y. Hu, R.K.K. Yuen, Influence of g-C3N4 nanosheets on thermal stability and mechanical properties of biopolymer electrolyte nanocomposite films: a novel investigation, ACS Appl. Mater. Interfaces 6 (1) (2014) 429–437.
[46] S.K. Gaddam, R. Pothu, R. Boddula, Graphitic carbon nitride (g-C3N4) reinforced polymer nanocomposite systems—a review, Polym. Compos. 41 (2) (2020) 430–442.
[47] F. Cuétara-Guadarrama, M. Vonlanthen, K. Sorroza-Martínez, I. González-Méndez, E. Rivera, Photoisomerizable azobenzene dyes incorporated into polymers and dendrimers. Influence of the molecular aggregation on the nonlinear optical properties, Dyes Pigments 194 (2021), 109551.
[48] E. Agbovhimen Elimian, M. Zhang, Y. Sun, J. He, H. Jia, Harnessing solar energy towards synergistic photothermal catalytic oxidation of volatile organic compounds, Sol. RRL 7 (14) (2023), 2300238.
[49] D. Bari, N. Wrachien, G. Meneghesso, C. Andrea, R. Tagliaferro, T.M. Brown, A. Reale, A.D. Carlo, Study of the effects of UV-exposure on dye-sensitized solar cells, in: 2013 IEEE International Reliability Physics Symposium, IRPS), 2013, 4B.3.1-4B.3.7.
[50] Y. Xiao, C. He, Z.-F. Yang, E.-Q. Chen, H.-J. Lu, X.-H. Li, Y.-F. Tu, The shackling effect in cyclic azobenzene liquid crystal, Chin. J. Polym. Sci. 40 (6) (2022) 584–592.
[51] Z. Cheng, R. Yu, F. Wang, H. Liang, B. Lin, H. Wang, S. Hu, J. Tan, J. Zhu, Y. Yan, Experimental study on the effects of light intensity on energy conversion efficiency of photo-thermo chemical synergetic catalytic water splitting, Therm. Sci. 22 (Suppl. 2) (2018) 709–718.
[52] A. El-Shaer, M. Tadros, M. Khalifa, Effect of light intensity and temperature on crystalline silicon solar modules parameters, International Journal of Emerging Technology and Advanced Engineering 4 (8) (2014) 311–318.